JOURNAL OF APPLIED PHYSICS VOLUME 91, NUMBER 2 15 JANUARY 2002

Improved binary collision approximation ion implant simulators

J. M. Hernández-Mangas,[a] J. Arias, L. Bailón, M. Jaraíz, and J. Barbolla
Departamento Electricidad y Electrónica, Universidad de Valladolid, E-47011 Valladolid, Spain

(Received 30 May 2001; accepted for publication 10 October 2001)

An efficient binary collision approximation (BCA) ion implant code with good prediction capabilities for semiconductor materials (Si, GaAs, SiC) with only one fitting parameter for low implantation doses is presented. It includes specific interatomic potentials and recent improvements in physical models for inelastic stopping. A periodic *ab initio* full bond electron density for the target is used. Damage accumulation is supported using a modified Kinchin–Pease model [G. H. Kinchin and R. S. Pease, Rep. Prog. Phys. **18**, 1 (1955)]. Also, some of the BCA integration algorithms and target selection procedure have been refined. An algorithm commonly used for statistical noise reduction has been modified to also improve the noise reduction in the lateral and shallow zones. The agreement with experiments is good, even under channeling conditions and for different target materials. A comparison with experimental secondary ion mass spectroscopy results for several projectiles and targets is presented. © *2002 American Institute of Physics.*
[DOI: 10.1063/1.1424052]

I. INTRODUCTION

Ion implantation is one of the main processes used for the fabrication of modern integrated microelectronic devices, and it allows controlled doping of the active regions. Reliable prediction of dopant concentrations by simulations is of great importance to save both cost and time required by experiments.

Accurate knowledge of the three-dimensional profile of the implanted ions is crucial for current deep submicron devices because this distribution is closely related to the electrical characteristics of the final device desired. The ability to accurately predict lateral doping profiles as well as depth profiles in a computationally efficient manner is important for optimum design and fabrication of advanced devices. Also, dopant profiles implanted with high energies are needed to create retrograde wells. Channeling of projectiles into the target must be taken into account in physical models, because some projectiles (e.g., boron into silicon) present a strong channeling component.[1–4]

To be predictive for different materials and projectiles, a simulation code must be able to simulate different implant conditions like the angle, orientation, oxide layer, dose, etc. with the same set of adjustable parameters and models.

The ion implant simulator must also allow a trade-off between speed and accuracy.[5] All of these aspects have been studied by different groups and are now scattered across different simulation codes. In an effort to analyze the prediction capabilities and computational efficiency that can be attained with these models, we have incorporated them all into a single simulation code. The purpose of this article is, therefore, to first describe the models implemented and then present an analysis of the performance of the combined use of these models in terms of prediction capabilities and computational efficiency. We selected the binary collision approximation (BCA) to achieve this because, although the molecular dynamics (MD) technique is more accurate than BCA, it needs much longer calculation times. In addition, BCA methods can be refined to improve their accuracy to meet current needs.

Historically, researchers have used several modeling schemes to solve the problem of ion implantation. The choice of which depends on the material's characteristics, such as amorphous[6] or crystalline[7] targets, and also on the level of description of the problem: MD, BCA, transport equation, etc.

In the 1960s, Lindhard–Scharff–Schiott (LSS) theory[8,9] was introduced to model ion implantation. In this theory the total stopping power is calculated as the sum of two independent contributions: nuclear (elastic) and electronic (inelastic). Nuclear stopping was obtained by means of classical mechanics. Electronic stopping was assumed to be proportional to the ion velocity and it did not depend on either the direction of the ion or individual collisions. This is nonlocal stopping and the ion is seen as moving in a uniform electron gas. This model did not follow the ion trajectory into the target and did not take into account the crystalline properties of the target.

An improved model was created in 1974 by Robinson and co-workers[7,10,11] (the MARLOWE code). In this model a crystalline target material with BC approximation is considered. It uses a symmetrically spherical electron density [Ziegler–Biersack–Littmark (ZBL) density][6] that does not represent either the bonds of covalent targets or the low electron density at the interstitial zones. It also used integration algorithms that did not take into account the effect of neighboring atom potential energy. As a result, it had a low predictive capability, and it needed a number of fitting parameters to match the experiments. This code has been greatly modified by many authors (see, e.g., Refs. 1 and 12).

A third simulation scheme for ion implantation was developed by Ziegler, Biersack and Littmark[6] in 1985. It was a

[a]Electronic mail: jesman@ele.uva.es

 © 2002 American Institute of Physics

Downloaded 01 Apr 2002 to 128.8.92.86. Redistribution subject to AIP license or copyright, see http://ojps.aip.org/japo/japcr.jsp

BCA Monte Carlo method for amorphous targets. The projectile trajectory is statistically followed by randomly selecting a target atom, an impact parameter and a distance (mean free path). The elastic part of the collision was solved by classical mechanics and obtained the new position, direction and energy for both the projectile and the target atom. To shorten the calculation time it uses a magic formula that fits the equations that are solved. The inelastic contribution was estimated using Brandt and Kitagawa theory.[13] It had two terms: proton stopping in a uniform electron gas, and a scaling factor for heavier projectiles. The proton stopping was fitted through experimental data. This model works sensibly well for amorphous targets, but it cannot be employed for crystalline targets.

A highly modified MARLOWE code (UT-MARLOWE) was developed[1,14–16] at the University of Texas at Austin. It covered the most commonly used implant species in single crystal silicon with explicit dependence on the energy, dose, tilt and rotation angles, but the models used for stopping, damage, etc. are different depending on the species, energy range, etc. in order to match the experimental results.

The CRYSTAL-TRIM[2] code is a combination of the MARLOWE and TRIM codes that is fast with amorphous targets, but it uses many adjustable parameters[17] both for the electronic stopping and the damage model to cover all the implant species and conditions.

The University of Wien has developed VISTA-MCIMPL but it also needs many fitting parameters to match experiments. It implements a complex rare-event model.[18]

Other attempts to model ion implantation have been made using mixes of the ones cited above or using MD. Molecular dynamics is very time consuming (orders of magnitude more than BCA). However, in the near future, MD may be the technique of choice for very low energies.

Our starting point was the MARLOWE scheme[7] but it has been completely rewritten in C++.[12,19,20] A physical model with only one adjustable parameter[21] has been used for electronic stopping using a novel integration method. Also to speed up the simulator a new statistical noise reduction scheme has been implemented.

II. PHYSICAL MODELS

Projectiles are simulated following their complete trajectory as well as the trajectories of the recoils generated (full cascade development). The target material is modeled as crystalline, polycrystalline or amorphous.[7] For polycrystalline targets random rotation of the whole crystal is made before each ion implant. For amorphous, random rotation of the crystal is done before each collision.

Thermal vibrations are considered using a Debye temperature model. The root mean square (rms) amplitude of the thermal displacement varies with the target temperature as $A_{\rm rms}=12.063\,464[A(T)/(T_{\rm Debye}M)]^{1/2}$ where M is the atomic mass, $T_{\rm Debye}$ is the Debye temperature of the target obtained experimentally[22] and $A(T)$ is the Debye function.[23]

Projectiles lose their energy both elastically and inelastically by collisions with the atoms of the target material. The binary collision approximation, used here, considers only a collision with one target atom at a time. Simultaneous collisions are modeled through a combination of individual collisions[10] when needed (e.g., channeling conditions).

The scheme followed iteratively is (i) a search of target candidates (like in Ref. 7); (ii) calculation of each binary (individual) elastic collision; (iii) the selection of actual targets; (iv) calculation of nonlocal electronic losses for each binary collision, considering the three-dimensional (3D) periodic electron density following the asymptotic trajectories (tabulating this procedure with the actual trajectories would lead to too high a computational burden); (v) calculation of local electronic losses for simultaneous collision with all the targets; and finally (vi) energy and momentum conservation rules are applied and the projectile and targets are moved to their new positions. Specific explanations of these steps will be given next.

A. Elastic losses: Specific screening functions

The nuclear interaction between the incident projectile and the target atom is solved by classical mechanics.[24] Numerical integration of the movement equations for both particles is done. To speed up the implant simulation, a look-up table is calculated beforehand. A repulsive Coulombic screened potential is used. The screening function can be selected from among several universal and specific ones. By default a universal screening function of ZBL[6] is used.

Other universal screening functions (those of Bohr and Molière in Ref. 25, of Lenz–Jensen in Ref. 26, of Thomas–Fermi in Ref. 27) have been tested.[28] We use specific screening functions, when available, for each projectile–target combination obtained by *ab-initio* methods[6] (e.g., with the DMOL code[29]) to reduce the number of approximations used by the simulator. When no specific screening function is available the one best suited seems to be the ZBL. It has a mean error of 2.1% with respect to specific screening functions.[6]

B. Inelastic losses: Physical models

It was found to be necessary[21] to include inelastic energy loss due to collisions (local) and energy loss due to background electronic stopping (nonlocal) as two distinct mechanisms in order to obtain good simulation results for a range of channeling conditions.[28,30,31] It is not possible to assume that one of these processes is dominant and to fit it to accurately model energy losses for different implant energies and directions.

Nonlocal inelastic stopping accounts for the average energy loss of the ion as it travels along the interstitial volume of the target. It is due to the interaction between the nucleus of the projectile and the target's electrons. This electronic stopping is given by the modified Brandt–Kitagawa[13] theory with only one adjustable parameter,[4,32] r_s^0. This stopping is calculated as

$$S_{\rm nonlocal}=\int_{\rm trajectory}[Z_1^*(v,r_s^0)]^2 S_p(v,r_s)\,dx, \tag{1}$$

where Z_1^* represents the effective charge of the ion, S_p is the electronic stopping power for a proton and $r_s=[3/(4\pi\rho)]^{1/3}$ is the one-electron radius (ρ is the local elec-

Downloaded 01 Apr 2002 to 128.8.92.86. Redistribution subject to AIP license or copyright, see http://ojps.aip.org/japo/japcr.jsp

tron density). The r_s^0 value is related to the effective electron density of the target and depends on the ion–target combination.[4]

According to Brandt and Kittagawa the effective charge is defined as $Z_1^* = Z_1 \gamma(v, r_s^0)$ with

$$\gamma(v,r_s^0) = q(v) + C(r_s^0)[1-q(v)]\ln\left[1+\left(\frac{4\Lambda}{r_s^0}\right)^2\right], \quad (2)$$

where $q(v)$ is the ionization fraction, $C(r_s^0)$ depends weakly on the target, but can be approximated to 0.5 and

$$\Lambda = \frac{2a_0[1-q(v)]^{2/3}}{Z_1^{1/3}\{1-[1-q(v)]/7\}}, \quad (3)$$

where $a_0 = 0.240\,05$. The ionization fraction, $q(v)$, is dependent on the relative velocity between the ion and the target. A scaling variable, defined as $y_r = v/(v_B Z_1^{2/3})$ where v_B is the Bohr velocity, is used to match an experimentally measured $(3 \leqslant Z_1 \leqslant 92)$ curve for the ionization fraction[6,33] following a velocity criterion for stripping electrons $q = 1 - \exp(0.803 y_r^{0.3} - 1.3167 y_r^{0.6} - 0.381\,57 y_r - 0.008\,983 y_r^2)$.

We have tested[28] other formulas for the ionization fraction with a velocity criterion[13] or with an energy criterion,[34] but the best results have been obtained with the formula cited above.

Proton stopping depends on the local electron density that results from the crystalline structure of the target. For low energies, a numerical approximation to the model of Echenique *et al.*[35] is used. For high energies Bethe's model[36] is used.

For the electron density we use a three-dimensional electron charge distribution for crystalline silicon that includes the covalent tetrahedrical bonds calculated by the *ab initio* pseudopotential total energy method in the local density approximation.[37] For other target materials the electron density can be obtained in the same way.

Local inelastic energy loss stopping is related to close collisions and takes into account the electron–electron interaction between the projectile and target atoms. It is described by the modified Firsov theory[38,39] proposed by Beardmore and Gronbech-Jensen:[21] $\Delta E_i = \int_{\text{trajectory}} F_{ij} dr$ where

$$F_{ij} = \frac{2^{1/3}\hbar}{2\pi a_B}(\hat{v}_j - \hat{v}_i)\left[Z_A^2 I\left(\frac{Z_A^{1/3}\alpha R}{a}\right) + Z_B^2 I\left(\frac{Z_B^{1/3}(1-\alpha)R}{a}\right)\right], \quad (4)$$

with

$$I(W) = \int_W^\infty \frac{\Phi^2(x)}{x} dx \quad (5)$$

and $\alpha = [1+(Z_B/Z_A)^{1/6}]^{-1}$, $\Phi(x)$ being the universal screening function,[6] Z_A and Z_B the atomic numbers ($Z_A \geqslant Z_B$), R the atomic separation, $a = (9\pi^2/128)^{1/3} a_B$, and a_B the Bohr radius. As reported by Firsov,[39] at sufficiently high ion velocities the electrons of the two atoms will not have the time necessary for free interaction, and therefore the transfer of energy will diminish. Following Ref. 40 we have accounted for this fact by damping out the energy transfer beyond a critical velocity ($v_c = 0.7 v_B$, where v_B is the Bohr velocity), as

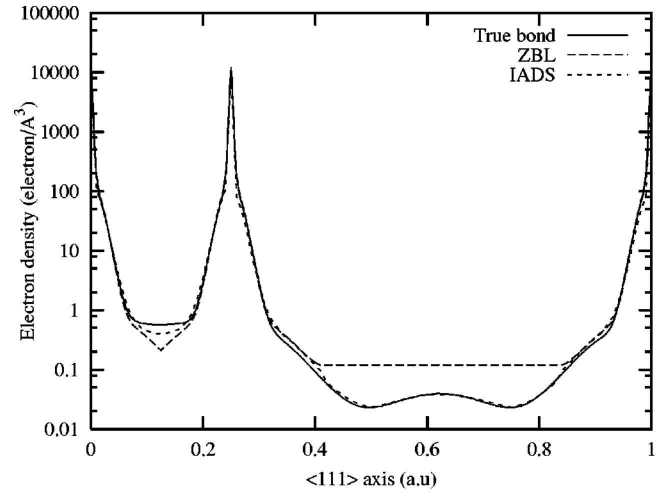

FIG. 1. Differences among ZBL, IADS and true bond densities along the {111} direction.

$$\Delta E_i^* = \Delta E_i \begin{cases} v/v_B, & \text{for } v < v_c, \\ v_c^2/(v v_B), & \text{for } v \geqslant v_c. \end{cases} \quad (6)$$

In order to obtain a smooth transition between the lower and upper velocity regions, the following transfer function[41] is used:

$$f(v) = \frac{2\exp[-(v/v_c)^2]}{1+\exp[-2(v/v_c)^2]}. \quad (7)$$

Finally, $S_{\text{local}} = f(v)\Delta E^*_{i,\text{low vel}} + (1-f(v))\Delta E^*_{i,\text{high vel}}$.

C. Three-dimensional electron density distribution

The local electron density distribution is also used for the calculation of nonlocal inelastic stopping. It is very important to match ends by periodicity to reduce the computation inaccuracies. The ZBL electron density is a spherically symmetric electron distribution calculated by Ziegler *et al.*[6] that was used by several authors.[4,17,42] It has a uniform interstitial density that does not represent the density of the open channels accurately (Figure 1). The 3D electron density used by us is obtained by means of the *ab initio* pseudopotential total energy method in the local density approximation.[37] It provides a full description of the covalent bonds of the target material. We have also used a 3D electron density that we call isolated atom density superposition (IADS). This approximation is closer to the true bond density than the ZBL one. We expected this should be a good approximation for nonpolar covalent materials (e.g., silicon).

Figure 1 shows the differences among ZBL, IADS and true bond densities along the {111} direction for a silicon target. It is clear that the ZBL density does not accurately represent some regions (in particular, interstitial regions).

A comparison of the ZBL, IADS, and full bond distributions[28,30,31] reveals the necessity for a three-dimensional description of the covalent nature of silicon.

Downloaded 01 Apr 2002 to 128.8.92.86. Redistribution subject to AIP license or copyright, see http://ojps.aip.org/japo/japcr.jsp

This necessity can be extended to other compound semiconductors which is even more important. For silicon targets the main differences observed were in the {110} channel direction.[28] Simulations without free parameters[43] have also proven the necessity of using a 3D electron density distribution.

D. Damage accumulation

In order to deal with high dose implantations the simulator must include some damage accumulation model. It is important especially in channeling cases. Although we have implemented full cascade development, due to practical reasons (mainly the speed of the simulator) we have begun implementing damage accumulation based on Kinchin–Pease theory[1,44] as a first approximation. In the near future we plan to include full cascade development in damage accumulation as a slower but more accurate option. Modeling of damage has two components: *defect generation/ recombination* and the *damage simulation*. The damage simulation will be described in Sec. III.

The number of point defects generated, n, is proportional to the energy, E, lost by nuclear scattering in each sector:

$$n=\frac{kE}{2E_d}, \tag{8}$$

where $k=0.8$ is a constant and E_d is the displacement threshold energy. For boron implantation into silicon $E_d=15$ eV. Part of the point defects generated recombines with other defects, so the net increase of point defects after recombination, Δn, is given by

$$\Delta n=nf_{\mathrm{surv}}\left(1-\frac{N}{N_\alpha}\right), \tag{9}$$

where f_{surv} is the fraction of point defects surviving both intracascade and intercascade recombination and it is adjusted for each kind of projectile implanted (e.g., $f_{\mathrm{surv}}=0.06$ for boron into silicon), N is the previous local defect density, and N_α is the local defect density necessary to reach amorphization (e.g., for silicon N_α is 10% of the atomic density).

III. COMPUTING ALGORITHMS

A. Inelastic losses: Integration methods

We have observed that the integration schemes for the two energy loss components can play a critical role in achieving the degree of accuracy demanded by current technology, particularly under channeling conditions. As a result, we use an integration method that is a hybrid between molecular dynamics and the BCA model in order to improve the numerical integrations.

For nonlocal electronic losses the straight projectile incoming trajectory is sampled (see Fig. 2, where straight movement is considered for the projectile between P_1 and P_2 and for the target from T_1 to T_2) having taken into account the potential energy at each point due to the surrounding neighbors, $E_p(x)$, the elastic energy transfer to the target, $E_T(x)$, and also the electronic losses accumulated up to this point, $S_{\mathrm{nonlocal}}(x)$. The local kinetic energy for the projectile is calculated as $E_c(x)=E_{c0}-E_T(x)-S_{\mathrm{nonlocal}}(x)-E_p(x)$ where E_{c0} is the initial kinetic energy at this collision. The $E_T(x)$ value is calculated by linear interpolation between its initial and final values. Since $v=\sqrt{2E_c/M_1}$ the nonlocal electronic losses can be integrated using Eq. (1).

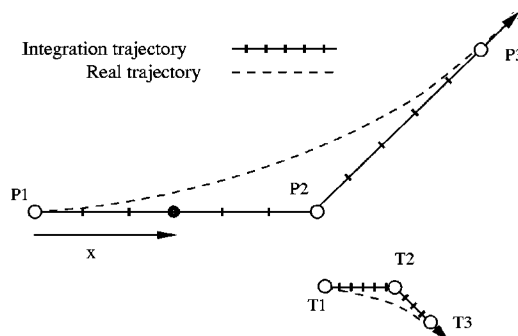

FIG. 2. Schematics for the local and nonlocal inelastic stopping integration algorithms.

The local inelastic losses are integrated along the straight incoming and outgoing trajectories (Fig. 2) of the projectile. Straight displacements are assumed for the target. At each point, the force F_{ij} between the projectile and the target is evaluated using Eq. (4). The outgoing trajectory is followed long enough to account for all the interaction. At this stage we consider the contributions of the electron densities of all the targets involved in the collision.

B. Statistical noise improvement algorithm

In order to reduce the calculation time and to improve the accuracy of the simulated profiles a three-dimensional rare event algorithm is implemented.[45] The straightforward way to obtain a statistically significant concentration at all depths of the profile is to run many simulated cascades. Most of the ions will stop near the main peak. The majority of computer effort will not improve the accuracy of the tail or low concentration zones. With the atom splitting scheme[45] at certain depths, the ion is split into two virtual ions with half statistical weight of an unsplit ion. The virtual ions generated have the same position and velocity as the parent ion. Their final trajectories are, however, different due to the thermal vibration effects. In the end, we obtain practically the same number of virtual ions at each bin of the histogram profile thereby improving the statistics in low concentration zones. In the ion implant simulation there are two rare event cases of particular interest that should be considered to improve the statistics of the impurity profile: the deep region (channeled ions) and the shallow region.

1. Channeled ions

The channeled ion case occurs when the projectile travels through a crystal channel. It loses its energy mainly by inelastic interaction without experiencing hard nuclear (elastic) collisions. We monitor the total distance traveled by the ion to improve statistics at both the deep and the lateral regions.

Downloaded 01 Apr 2002 to 128.8.92.86. Redistribution subject to AIP license or copyright, see http://ojps.aip.org/japo/japcr.jsp

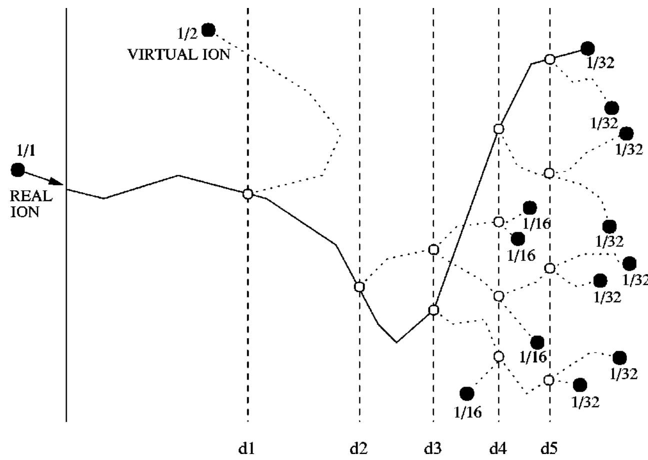

FIG. 3. Rare event algorithm with a lateral or depth enhancement scheme.

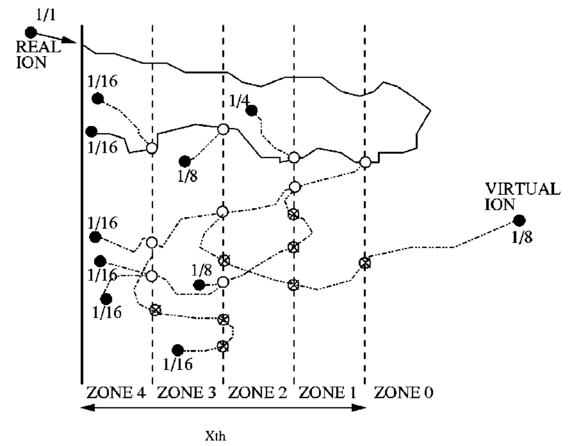

FIG. 5. Rare event algorithm with a shallow region enhancement scheme.

In general, we define a border d_i as either a depth reached by the ion or as the total distance traveled by the projectile. When the ion reaches the border with the next index, it is split into two virtual ions with half the statistical weight. Figure 3 shows an example of how a real ion is split several times into several virtual ions when it reaches certain borders. We also show the statistical weight associated with each virtual ion. The borders cited above are calculated by solving the following equation:

$$\int_0^{d_i} C(x)dx = (1-(1/2)^i)\int_0^{\infty} C(x)dx, \tag{10}$$

where $C(x)$ is the dopant histogram profile at a certain depth (or total distance traveled) x.

With this scheme we can recalculate the splitting borders dynamically in order to improve the statistics in specific regions. We do not need to know the borders *a priori*. First, N_0 real ions are simulated without the rare event algorithm, to obtain some statistics to estimate the initial borders d_i. Then, the algorithm is activated and the borders are recalculated every N_{interval} real ions. This value must be large enough (e.g., $N_{\mathrm{interval}} = 100$) so that the computation time is not increased noticeably. When we have attained the desired statistical accuracy in the rare event region, the algorithm is automatically deactivated.

Figure 4 shows the dopant profiles obtained for implantation of boron into silicon with 2 keV, with and without the trajectory-length selection scheme. We observe better definition of the profile tail. The simulation time is doubled using the algorithm, but the time needed to obtain the same accuracy without the algorithm would have been 10 times longer.[45]

2. Projectiles in the shallow region of the impurity profile

When we simulate medium and high energy implants there is some statistical noise in the shallow region of the profiles due to the (few) ions that have lost their energy at the beginning of their trajectory. We use two conditions to identify these projectiles.

First, an energetic condition: the energy decreases below a user defined threshold energy, $E \leq E_{\mathrm{th}}$, that is generally a percentage of the initial energy. Ions that verify this condition are likely to stop nearby.

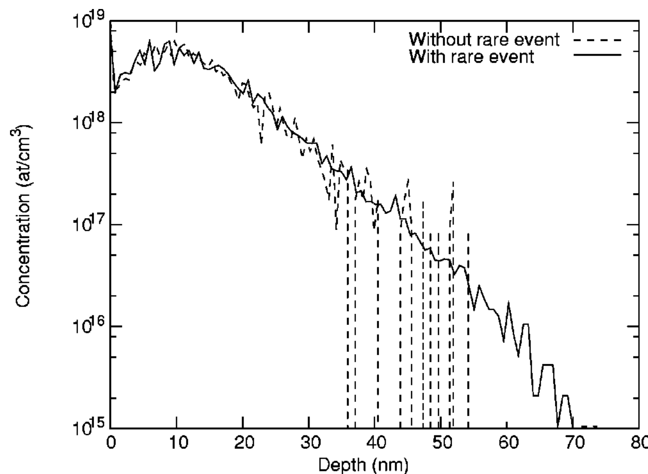

FIG. 4. Implantation of B (tilt=7°, rotation=30°) → Si {100}, 2 keV simulated with $N_{\mathrm{ion}} = 2000$ real ion with and without the trajectory-length selection scheme.

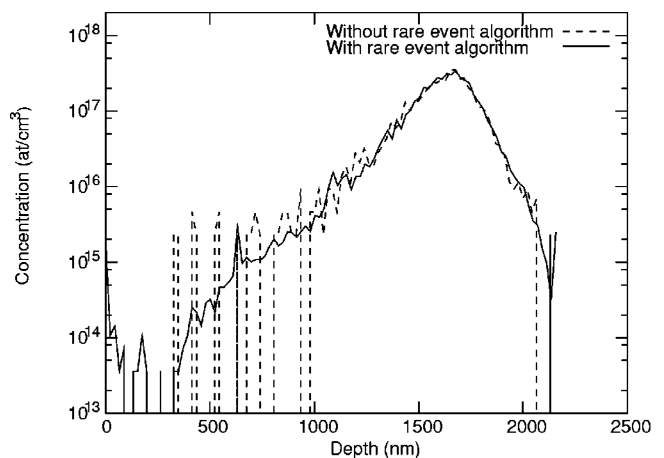

FIG. 6. Comparison of profiles of an implantation of B (7°, 30°) → Si {100}, 1 MeV simulated with $N_{\mathrm{ion}} = 2000$ real ions with and without the shallow region enhancement scheme.

Downloaded 01 Apr 2002 to 128.8.92.86. Redistribution subject to AIP license or copyright, see http://ojps.aip.org/japo/japcr.jsp

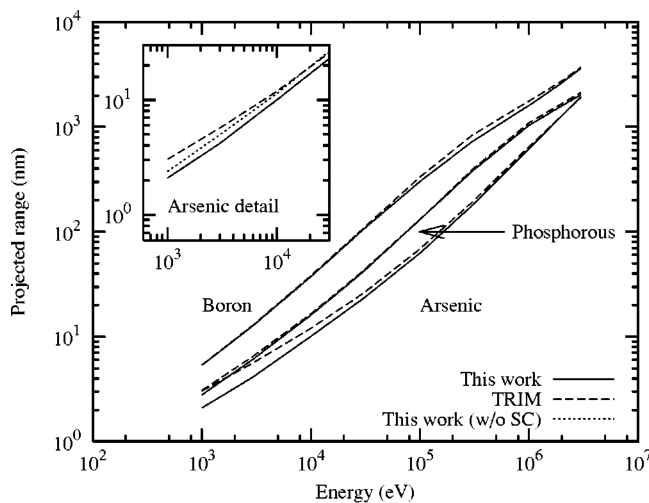

FIG. 7. Boron, phosphorus and arsenic implanted into amorphous silicon. Comparison between simulation results of TRIM and this work. The inset shows the differences found with and without the simultaneous collision (SC) treatment for arsenic.

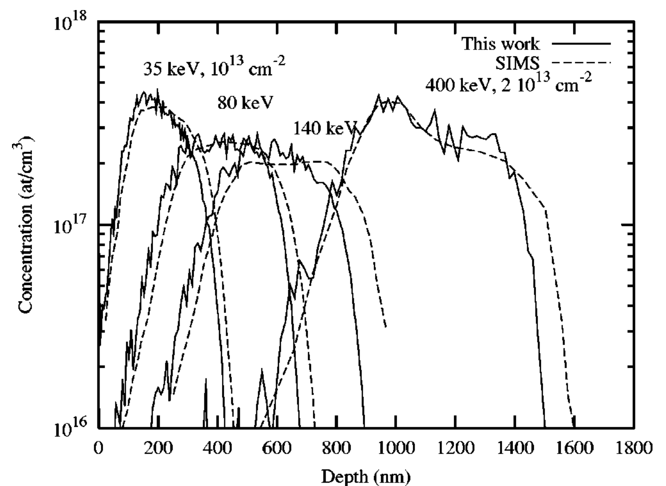

FIG. 9. Comparison of boron (0°, 0°) with 35 and 80 keV and boron (0.6°, 0°) with 140 and 400 keV implants into {100} silicon (with a 15 Å SiO_2 layer, 0.5° divergency) between SIMS profiles (Refs. 4 and 48) and the simulation results in this work.

Second, a position condition: we consider the shallow region (Fig. 5) defined by $W_{\text{shallow}} = p_d(D_{\max} - D_{\min})$, where $D_{\max}$ is the maximum depth reached by an implanted ion, $D_{\min}$ is the positive minimum depth of the current profile and p_d is the percentage of the whole profile that the user considers to be the shallow region. We divide W_{shallow} into N equal zones. Initially the projectile is considered to have an index of 0 ($n_{\text{index}} = 0$, with unity statistical weight). When the first condition ($E \leqslant E_{\text{th}}$) is met we compare the current depth of the projectile, $D_{\text{projectile}}$, with the border that defines the next index as $D_{\text{projectile}} < D_{\min} + W_{\text{shallow}}(1 - n_{\text{index}}/N)$.

If the two conditions are met we split the current ion into two virtual half-weighted ions and we increase n_{index}. Then the same procedure is applied to both virtual ions again. Finally, the algorithm is deactivated when the statistical accuracy required is reached.

Figure 6 shows a retrograde implant profile of boron into silicon with and without the shallow region enhancement scheme. We want to note the better definition of that region. The simulation time is increased 50% with respect to not using the algorithm, but the time necessary to obtain the same statistical accuracy by increasing the number of projectiles simulated (by 10), increases the time by a factor of 7.6 in this case.[45]

C. Damage accumulation

As defined above our damage model is based on the modified Kinchin–Pease model[1,44] and its modeling has two components: *defect generation/recombination* and the *damage simulation*. Surface recessing by sputtering is not accounted for in this simulator but this effect is negligible in the examples shown.

For defect generation/recombination, in one-dimensional (1D), the crystal is divided into slices perpendicular to the depth axis. Equations (8) and (9) are applied to each sector to calculate its defect density. To reduce the computational

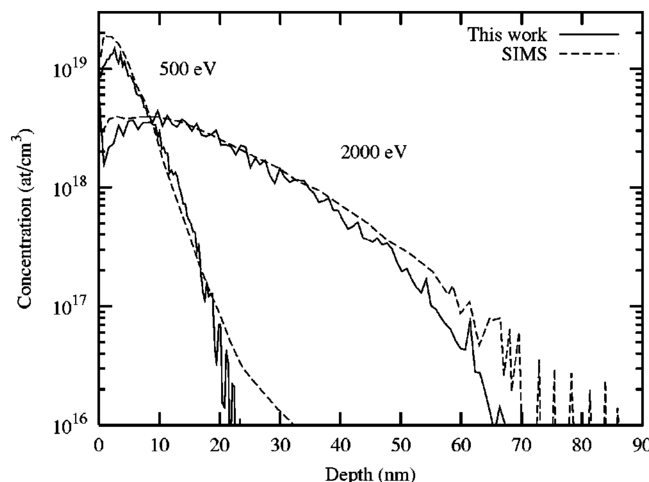

FIG. 8. Comparison of boron (0°, 0°) into a {100} silicon implant (500 and 2000 eV) between SIMS profiles (Ref. 21) and the simulation results in this work.

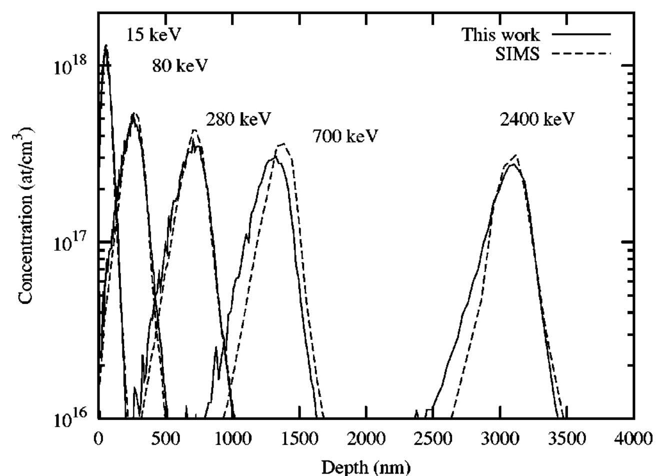

FIG. 10. Comparison of boron (7°, 30°) into {100} silicon implant (15, 80, 280, 700 and 2400 keV, with a 15 Å SiO_2 layer) between SIMS profiles (Refs. 4 and 16) and the simulation results in this work.

Downloaded 01 Apr 2002 to 128.8.92.86. Redistribution subject to AIP license or copyright, see http://ojps.aip.org/japo/japcr.jsp

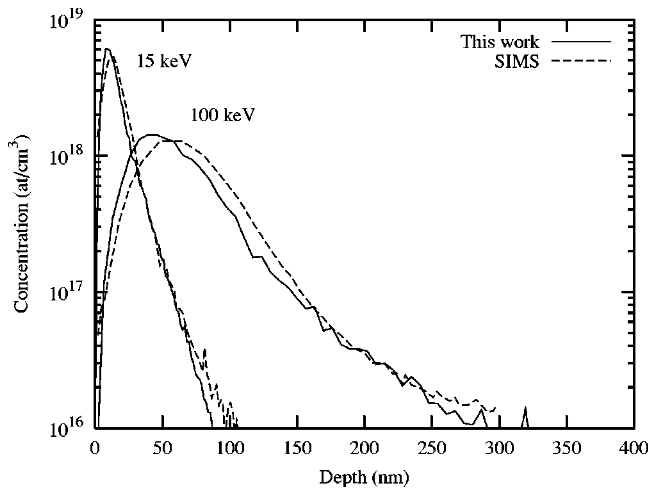

FIG. 11. Comparison of arsenic (8°, 30°) with 15 and 100 keV into {100} silicon implant between SIMS profiles (Ref. 32) and the simulation results in this work.

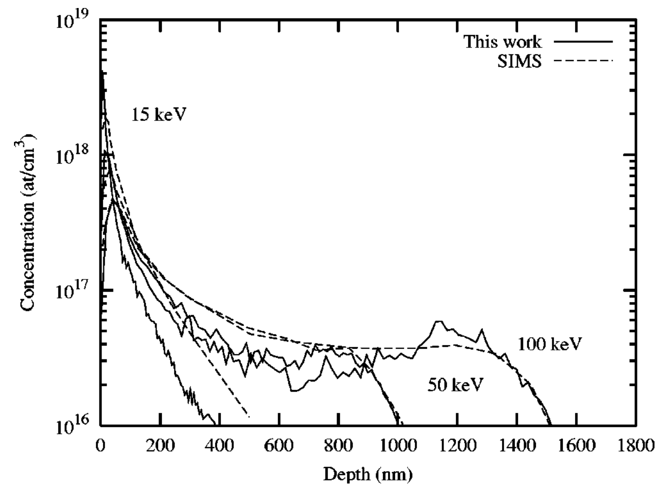

FIG. 13. Comparison of arsenic (0°, 0°) with 15, 50 and 100 keV into {110} silicon implant between SIMS profiles (Ref. 16) and the simulation results in this work.

overload generated by following the complete cascade simplification can be used.[15,44] The simulator considers only the primary ion. When a scattering event occurs the energy transferred to the target atom E_T is compared to a cut-off energy (e.g., $E_{\mathrm{cutoff}}=24$ eV, for boron into silicon). If E_T is greater than the cutoff energy then the algorithm considers only a transfer energy of $E_T=E_{\mathrm{cutoff}}$. This energy is defined as the energy needed to completely amorphize a sector as the result of a single collision. This approximation does not take into account the energy deposited by secondary atoms. The reduction in calculation time using this approximation is about 30%. The N_α and f_{surv} parameters depend on the E_{cutoff} value.

In the damage simulation, for a given dose Φ, we define the area of the sectors as $A=N_{\mathrm{ions}}/\Phi$, where N_{ions} is the total number of real ions to be simulated. We apply periodic boundary conditions at the lateral borders of each sector. The local defect density, N, is a measure of the amorphization of each sector in the crystal. If the sector is completely amorphous, a random rotation of the crystal lattice is performed for each collision just like in MARLOWE.[7] For a partially amorphized section the rotation probability is N/N_α. After collision, the original crystal orientation is restored.

D. Speeding up the calculation

Several strategies have been employed throughout the code to speed up the calculation. When possible, look-up tables[12] calculated beforehand are used: elastic interaction, local and nonlocal inelastic losses, etc. The tables are calculated and stored on a disk for future use for each projectile–target atom combination.

E. Selection of the target atoms

The BCA needs a method with which to select the next target atoms to collide with. We began by using the MARLOWE[7] target atom selection method. It accepts target atoms that are in the direction of ion movement and have an

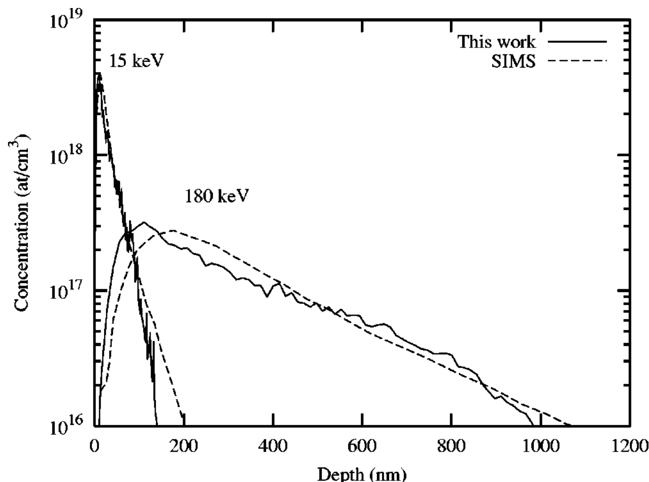

FIG. 12. Comparison of arsenic (0°, 0°) with 15 and 180 keV into {100} silicon implant between SIMS profiles (Ref. 32) and the simulation results in this work.

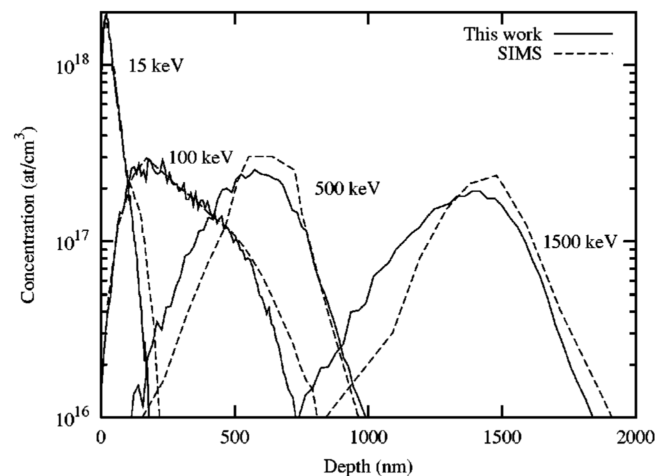

FIG. 14. Comparison of phosphorus (0°, 0°) with 15 and 100 keV and phosphorus (10°, 15°) with 500 and 1500 keV into {100} silicon implant between SIMS profiles (Ref. 21) and the simulation results in this work.

Downloaded 01 Apr 2002 to 128.8.92.86. Redistribution subject to AIP license or copyright, see http://ojps.aip.org/japo/japcr.jsp

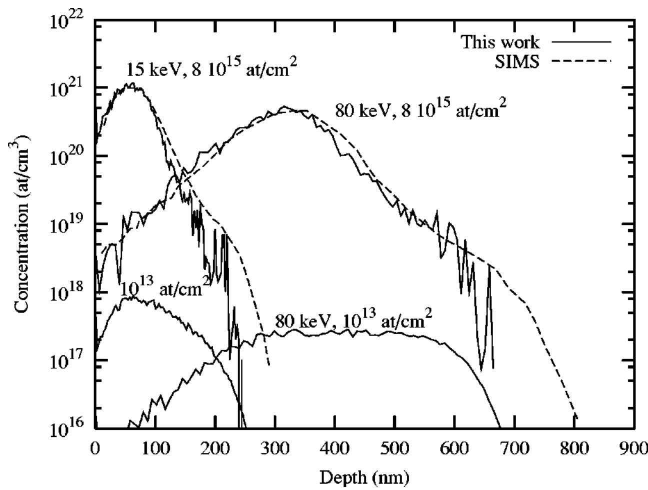

FIG. 15. Comparison of high dose, 8×10^{15} atoms/cm^2, boron (0°, 0°) with 15 and 80 keV into {100} silicon implant between SIMS profiles (Ref 16) and the simulation results in this work. Note the differences with the low dose simulation results.

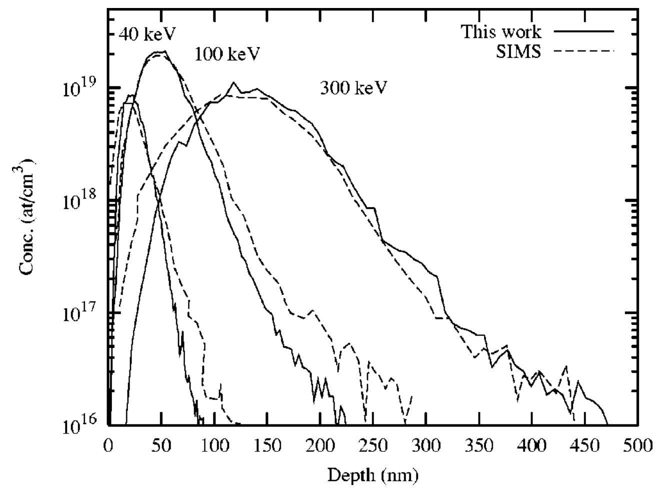

FIG. 17. Arsenic (12.5°, 30°) into 6*H*-SiC, 40, 100 and 300 keV implants with doses of 2×10^{13}, 9.9×10^{13} and 1.1×10^{14} atoms/cm^2, respectively. The orientation of the wafer flat is {11$\bar{2}$0} and the wafers are cut 3.5° off axis from the {0001} plane toward the {11$\bar{2}$0} direction (Ref. 46).

impact parameter that is smaller than a given value ($p < p_{\max}$) and a front distance $\xi > \xi_{\min}$, where $\xi_{\min}$ was obtained from the last collision[11] to prevent successive collisions with the same target atom. After we verify, step by step.There was identical behavior between MARLOWE and our simulator in selecting the target atoms. At this point, we observed that, randomly, the selection mechanism missed a target atom or recollided with the same atom. This is due to thermal vibrations that displace the target atom from its lattice position. To avoid this incorrect behavior that primarily modifies the channeling tail, we compiled a list with the atoms involved in the last collision. We compared the new targets with the old ones, and removed the ones that were repeated. This replaces the $\xi_{\min}$ condition.

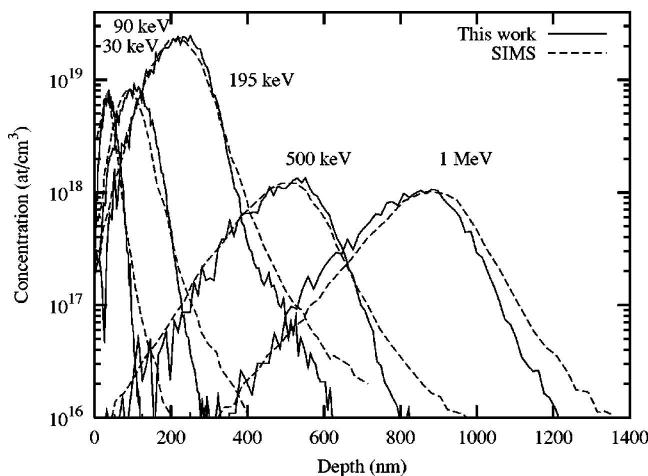

FIG. 16. Aluminum (12.5°, 30°) into 6*H*-SiC, 30, 90, 195, 500 and 1000 keV implants with doses of 3×10^{13}, 7.9×10^{13}, 3.8×10^{14}, 3×10^{13}, and 3×10^{13} atoms/cm^2, respectively. The orientation of the wafer flat is {11$\bar{2}$0} and the wafers are cut 3.5° off axis from the {0001} plane toward the {11$\bar{2}$0} direction (Ref. 46).

IV. RESULTS

We now compare simulated dopant profiles with experimental ones or with results from other simulators in order to assess our implementation of the ion implant BCA simulation and to test its prediction capabilities.

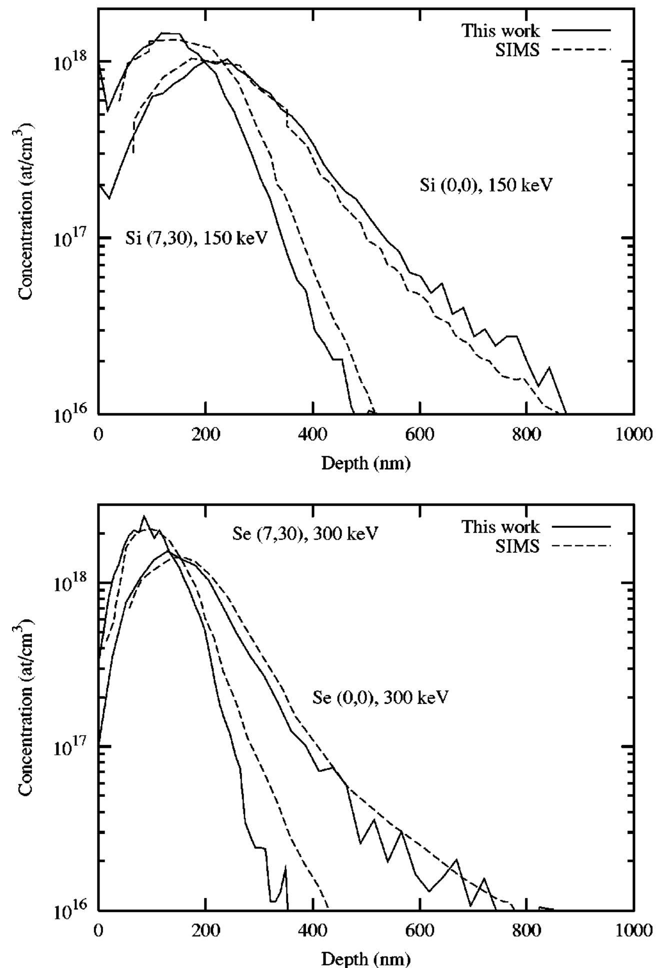

FIG. 18. (Top) Silicon at 150 keV and (bottom) selenium at 300 keV (REO and {100} channel) implanted after (Ref. 47) into GaAs.

Downloaded 01 Apr 2002 to 128.8.92.86. Redistribution subject to AIP license or copyright, see http://ojps.aip.org/japo/japcr.jsp

A. Silicon target

We first compare our simulation results with results from the well-known, validated TRIM amorphous simulator.[6] Since the profile shape is the same, Fig. 7 shows only the projected range versus the projectile energy for boron, arsenic and phosphorus implants into amorphous silicon. Very good agreement is obtained. Simultaneous collision treatment is necessary to correctly simulate[10] the channeling effect in crystalline targets. Since TRIM was designed for amorphous materials, it does not include this kind of treatment. However, at low velocities, there are simultaneous collisions even in amorphous materials. This leads to underestimation of stopping by TRIM that is more relevant at low velocities (heavy ions, low energies), as can be seen in the inset of Fig. 7 for As.

For crystalline targets we compare our simulation results directly with secondary ion mass spectroscopy (SIMS) experimental profiles obtained from the literature.[16,21,32,42] Figures 8–10 show boron implanted into silicon for several energies and implant conditions and they show good agreement with experiments that include very low energy (Fig. 8), channeling conditions (Fig. 9) and high energy (Fig. 10). All implants use the same (and only) fitting parameter $r_s^0 = 1.85$.

Figures 11–13 show implants of arsenic into silicon for several energies and implant conditions. For this ion–target combination we use $r_s^0 = 2.0$ for all conditions.

In Fig. 14 we see phosphorus into silicon implants also with several energies and implant conditions. The value employed for r_s^0 is 1.85, identical to that in the boron–silicon case.

Figure 15 shows a high dose, 8×10^{15} atoms/cm^2, boron into silicon implants for 15 and 80 keV and gives good agreement with the SIMS profiles.

These examples show the prediction capabilities of the models implemented in our simulator for a wide range of implant conditions (orientation, energy, etc.). To be able to simulate a new ion species only one fitting parameter, r_s^0, would have to be optimized.

B. Silicon carbide target

To further check the prediction capabilities of our model, we show some implant examples of implantation into 6*H*-SiC with several projectiles. Ion implantation is almost the only current method with which to dope silicon carbide. We used the IADS electron density approach so we only fitted the r_s^0 parameter.

Figure 16 shows an aluminum implant into 6*H*-SiC. The tilt angle is 12.5° and the rotation is 30°. The orientation of the wafer flat is $\{11\bar{2}0\}$ and the wafers are cut 3.5° off axis from the $\{0001\}$ plane toward the $\{11\bar{2}0\}$ direction. We compare the simulation results of 30, 90, 195, 500 and 1000 keV aluminum implants with the SIMS experimental[46] profile. Very good agreement is found. For Al into SiC we use $r_s^0 = 1.70$, which is not too different from the values used for the silicon target implants. We use the same damage accumulation parameters as those for silicon.

Figure 17 represents 40, 100 and 300 keV arsenic implants into 6*H*-SiC using the same conditions cited above ($r_s^0 = 1.75$). Again, they match very well.

C. Other target materials

Other interesting semiconductor materials are III–V semiconductors, like gallium arsenide. Special characteristics of this material are a very low Debye temperature (360 K) and softness. Damage accumulation is important even for low doses ($N_\alpha = 6\times10^{20}$ atoms/cm^3, $f_{\mathrm{surv}} = 0.09$).

Figure 18 shows silicon into GaAs [random equivalent orientation (REO)] and {100} channel, ($r_s^0 = 2.0$) implants at 150 keV, 3×10^{13} atoms/cm^2 compared with SIMS profiles[47], and it shows a comparison between selenium into GaAs (REO and {100} channel, $r_s^0 = 1.7$) implants at 300 keV, 3×10^{13} atoms/cm^2, and SIMS profiles.[47]

V. CONCLUSIONS

A BCA ion implant simulator was reported. It gathers some of the best physical models and simulation algorithms, including a hybrid integration scheme for inelastic energy losses. It also uses an *ab initio* physical description of the electron distribution for target atoms. For low implant doses, the simulator is capable of predicting the impurity implant profiles for a wide range of projectile atoms and target materials with only one adjustable parameter (r_s^0) for each projectile–target material combination. For high doses, there are two additional fitting parameters (f_{surv} and N_α).

ACKNOWLEDGMENTS

This work was performed under the auspices of the Junta de Castilla y León (Grant No.1 VA 14/00B) and DGICYT Project No. PB 98-0398.

[1] K. M. Klein, C. Park, and A. F. Tasch, IEEE Trans. Electron Devices **39**, 1614 (1992).
[2] M. Posselt, Radiat. Eff. Defects Solids **130**, 87 (1994).
[3] C. S. Murthy and G. R. Srinivasan, IEEE Trans. Electron Devices **39**, 264 (1992).
[4] D. Cai, N. Gronbech-Jensen, C. M. Snell, and K. M. Beardmore, Phys. Rev. B **54**, 17147 (1996).
[5] *International Technology Roadmap for Semiconductors* (Semiconductor Industry Association, San Jose, CA, 1999).
[6] J. F. Ziegler, J. P. Biersack, and U. Littmark, *The Stopping and Range of Ions in Solids* (Pergamon, New York, 1985).
[7] M. T. Robinson and I. M. Torrens, Phys. Rev. B **9**, 5008 (1974).
[8] J. Lindhard and M. Scharff, Phys. Rev. **124**, 128 (1961).
[9] J. Lindhard, M. Scharff, and H. E. Schiott, Dan. Vidensk. Seksk. Mat. Fys. Medd. **33**, 1 (1963).
[10] M. Hou and M. T. Robinson, Nucl. Instrum. Methods **132**, 641 (1976).
[11] M. T. Robinson, Phys. Rev. B **40**, 10717 (1989).
[12] J. Arias, M. Jaraiz, L. Pelaz, L. Bailón, and J. Barbolla, Nucl. Instrum. Methods Phys. Res. B **102**, 228 (1995).
[13] W. Brandt and M. Kitagawa, Phys. Rev. B **25**, 5631 (1982).
[14] S. H. Yang, S. Morris, S. Tian, K. Karab, A. F. Tasch, P. M. Echenique, R. Capaz, and J. Joannopoulos, Mater. Res. Soc. Symp. Proc. **389**, 77 (1995).
[15] G. Wang, S. Tian, M. Morris, B. Obradovich, G. Balamurugan, and A. Tasch, Proc. SPIE **3231,** 324 (1997).
[16] University of Texas at Austin, 1999; http://homer.mer.utexas.edu/TCAD/utmarlowe.
[17] M. Posselt, B. Schmidt, T. Feudel, and N. Strecker, Mater. Sci. Eng., B **71**, 128 (2000).

Downloaded 01 Apr 2002 to 128.8.92.86. Redistribution subject to AIP license or copyright, see http://ojps.aip.org/japo/japcr.jsp

[18] W. Bohmayr, A. Burenkov, J. Lorenz, H. Ryssel, and S. Selberherr, IEEE Trans. Semicond. Manuf. **8**, 402 (1995).
[19] J. Arias, M. Jaraiz, J. E. Rubio, L. Pelaz, L. A. Marqués, and J. Barbolla, J. Mater. Sci. Technol. **11**, 1191 (1995).
[20] J. Arias, J. Hernández, M. Jaraiz, L. Bailón, and J. Barbolla, in *Conferencia de Dispositivos Electrónicos*, Barcelona, 1997.
[21] K. M. Beardmore and N. Gronbech-Jensen, Phys. Rev. E **57**, 7278 (1998).
[22] G. Buschhorn, E. Diedrich, W. Kufner, M. Rzepka, H. Genz, P. Hoffmann-Stascheck, and A. Richter, Phys. Rev. B **55**, 6196 (1997).
[23] C. Kittel, *Introducción a la Física del Estado Sólido* (Reverté, Barcelona, 1993).
[24] J. B. Marion, *Classical Dynamics of Particles and Systems* (Academic, New York, 1986).
[25] G. Moliere, Z. Naturforsch. A **A2**, 133 (1947).
[26] W. Lenz, Z. Phys. **77**, 713 (1947).
[27] A. Sommerfeld, Z. Phys. **77**, 722 (1932).
[28] J. Hernández, Ph.D. thesis, University of Valladolid, Valladolid, Spain, 2000.
[29] DMOL is a trademark of Bio Sym Inc., San Diego, CA.
[30] J. Hernández, M. Jaraiz, J. Arias, L. Bailón, J. Barbolla, A. Rubio, and J. L. Orantes, *Conferencia de Dispositivos Electrónicos*, Madrid, 1999.
[31] J. Hernández, M. Jaraiz, J. Arias, J. Barbolla, L. Bailón, and A. Rubio, *Materials Research Society Spring Meeting*, San Francisco, 1998.
[32] D. Cai, C. M. Snell, K. M. Beardmore, and N. Gronbech-Jensen, Int. J. Mod. Phys. C **9**, 459 (1998).
[33] S. Kreussler, C. Varelas, and W. Brandt, Phys. Rev. B **23**, 82 (1981).
[34] R. J. Mathar and M. Posselt, Phys. Rev. B **51**, 107 (1995).
[35] P. M. Echenique, R. M. Nieminen, and R. H. Ritchie, Solid State Commun. **37**, 779 (1981).
[36] H. A. Bethe, Ann. Phys. (N.Y.) **5**, 325 (1930).
[37] A. Rubio, Dpto. Física Teórica, Facultad de Ciencias, Univ. de Valladolid, 1997 (private communication).
[38] L. M. Kishinevskii, Bull. Acad. Sci. USSR, Phys. Ser. (Engl. Transl.) **26**, 11433 (1962).
[39] O. B. Firsov, Sov. Phys. JETP **36**, 1076 (1959).
[40] S. Morris, D. Lin, S. H. Yang, S. Tian, K. Parab, and A. F. Tasch, Mater. Res. Soc. Symp. Proc. **396**, 27 (1996).
[41] M. J. Dort, P. H. Woerlee, and A. J. Walker, Solid-State Electron. **37**, 411 (1994).
[42] K. M. Klein, C. Park, and A. F. Tasch, Nucl. Instrum. Methods Phys. Res. B **59/60**, 60 (1991).
[43] J. Sillampäa, K. Nordlund, and J. Keinonen, Phys. Rev. B **62**, 3109 (2000).
[44] G. H. Kinchin and R. S. Pease, Rep. Prog. Phys. **18**, 1 (1955).
[45] J. M. Hernández-Mangas, J. Arias, M. Jaraíz, L. Bailón, and J. Barbolla, Nucl. Instrum. Methods Phys. Res. B **174**, 433 (2001).
[46] S. Ahmed, C. J. Barbero, T. W. Sigmon, and J. W. Erickson, J. Appl. Phys. **77**, 6194 (1995).
[47] R. G. Wilson and V. R. Deline, Appl. Phys. Lett. **37**, 793 (1980).
[48] P. Packman, H. Kennel, S. Thompson, S. Corcoran, and M. Taylor, in Proceedings of the *11th International Conference on Ion Implantation Technology, 1997*, edited by E. Ishida, S. Banerjee, S. Mehta, T. C. Smith, M. Current, and L. Larson (Institute of Electrical and Electronics Engineers, Piscataway, NJ, 1997), pp. 539–542.

Downloaded 01 Apr 2002 to 128.8.92.86. Redistribution subject to AIP license or copyright, see http://ojps.aip.org/japo/japcr.jsp